Compact electro-optic modulator on silicon-on-insulator substrates using cavities with ultra-small modal volumes

Bradley Schmidt, Qianfan Xu, Jagat Shakya, Sasikanth Manipatruni, and Michal Lipson

School of Electrical and Computer Engineering,
Cornell University, 414 Phillips Hall, Ithaca, NY 14853-5401
lipson@ece.cornell.edu

Abstract: We experimentally demonstrate a micron-size electro-optic modulator using a high-index-contrast silicon Fabry-Pérot resonator cavity. This compact device consists of a 1-D cavity formed within a single mode silicon channel waveguide and an embedded p-i-n junction on a silicon-on-insulator platform. The entire device is 6.0 microns in length. We demonstrate modulation depths as large as 5.87 dB at speeds of 250 Mbps limited only by fabrication imperfections, with optimized theoretical speeds of several Gbps.

References and Links

1. A. Liu, R. Jones, L. Liao, D. Samara-Rubio, D. Rubin, O. Cohen, R. Nicolaescu, and M. Paniccia, "A high-speed silicon optical modulator based on a metal-oxide-semiconductor capacitor," Nature **407**, 615-619 (2004).
2. A. Huang, G. Li, Y. Liang, S. Mirsaidi, A. Narasimha, T. Pinguet, and C. Gunn, "A 10Gb/s photonic modulator and WDM MUX/DEMUX integrated with electronics in 0.13µm SOI CMOS," presented at 2006 IEEE International Solid-State Circuits Conference, San Francisco, CA, USA, 2006.
3. T. Sadagopan, S. J. Choi, S. J. Choi, P. D. Dapkus, and A. E. Bond, "Optical modulators based on depletion width," IEEE Photon. Technol. Lett. **17**, 567-569 (2005).
4. R. D. Kekatpure, R. S. Shenoy, and M. L. Brongersma, "Design of a silicon-based field-effect electro-optic modulator with enhanced light-charge interaction," Opt. Lett. **30**, 2149-2151 (2006).
5. C. E. Png, J. Sun, and E. P. Li, "Tunable and sensitive biophotonic waveguides based on photonic-bandgap microcavities," presented at 2006 IEEE Conference on Emerging Technologies – Nanoelectronics, Singapore, 2006.
6. R. A. Soref and J. P. Lorenzo, "All-silicon active and passive guided-wave components for λ =1.3 and 1.6µm," IEEE J. Quantum Electron. **22**, 6, 873-879 (1986).
7. R. A. Soref and B. R. Bennett, "Electrooptical effects in silicon," IEEE J. Quantum Electron. **23**, 123-129 (1987).
8. Q. Xu, B. Schmidt, S. Pradhan, and M. Lipson, "Micrometre-scale silicon electro-optic modulator," Nature **435**, 325-327 (2005).
9. B. G. Lee, B. A. Small, K. Bergman, Q. Xu, and M. Lipson, "Transmission of high-data-rate optical signals through a micrometer-scale silicon ring resonator," Opt. Lett. **31**, 2701-2703 (2006).
10. J. S. Foresi, P. R. Villeneuve, J. Ferrera, E. R. Thoen, G. Steinmeyer, S. Fan, J. D. Joannopoulos, L. C. Kimerling, H. I. Smith, and E. P. Ippen, "Photonic-bandgap microcavities in optical waveguides," Nature **390**, 143-145 (1997).
11. A. S. Jugessur, P. Pottier, and R. M. de La Rue, "Engineering the filter response of photonic crystal microcavity filters," Opt. Express **12**, 1304-1312 (2004).
12. P. Lalanne, S. Mias, and J. P. Hugonin, "Two physical mechanisms for the boosting the quality factor to cavity volume ratio of photonic crystal microcavities," Opt. Express **12**, 458-467 (2004).
13. P. Velha, J. C. Rodier, P. Lalanne, and J. P. Hugonin, "Ultracompact silicon-on-insulator ridge-waveguide mirrors with high reflectance," Appl. Phys. Lett. **89**, 171121 (2006).
14. C. A. Barrios, V. R. Almeida, and M. Lipson, "Low-power-consumption short-length and high-modulation-depth silicon electrooptic modulator," IEEE J. of Lightwave Technol. **21**, 1089-1098 (2003).

15. C. A. Barrios, V. R. Almeida, R. Panepucci, and M. Lipson, "Electrooptic modulation of silicon-on-insulator submicrometer size waveguide devices," IEEE J. of Lightwave Technol. **21**, 2332-2339 (2003).
16. B. Jalali, O. Boyraz, D. Dimitropoulos, and V. Raghunathan, "Scaling laws of nonlinear silicon nanophotonics," Proc. SPIE **5730**, 41-51 (2005).
17. V. R. Almeida, R. R. Panepucci, and M. Lipson, "Nanotaper fro compact mode conversion," Opt. Lett. **28**, 1302-1304 (2003).
18. Q. Xu, B. Schmidt, J. Shakya, and M. Lipson, "Cascaded silicon micro-ring modulators for WDM optical interconnection," Opt. Express **14**, 9430-9435 (2006).
19. V. R. Almeida, C. A. Barrios, R. R. Panepucci, and M. Lipson, "All-optical control of light on a silicon chip," Nature, **431**, 1081-1084 (2004).
20. S. F. Preble, V. R. Almedia, and M. Lipson, "Optically controlled photonic crystal nanocavity in silicon," Proc. SPIE **5511**, 10-17 (2004).
21. M. S. Nawrocka, T. L. Wang, and R. R. Panepucci, " Tunable silicon microring resonator with wide spectral range," Appl. Phys. Lett. **89**, 071110 (2006).

1. Introduction

The realization of small-scale optical interconnects relies on the ability to integrate micro-optical devices with microelectronics. Electro-optic (E-O) modulators have recently been proposed and demonstrated with high performance [1-5]. In silicon, these devices rely on the relatively weak free carrier dispersion effect [6,7], and therefore are typically long and require high driving powers for obtaining a significant modulation depth. More compact modulators based on micron-sized ring resonators with diameters of 10-15 microns and high quality factor Q were recently demonstrated [8]. For on-chip high density optical interconnects that may require tens of thousands of electro-optic devices integrated on chip, however, extremely low power and small-size devices are needed. The power could be reduced by using resonators with even higher Q's, which increases the sensitivity of the device to small index changes. The corresponding reduced bandwidth of such resonators, however, becomes impractical as a result of distortion of the bits of data as the optical lifetime inside the cavity approaches the time per bit passing through the device [9].

Ultra-small cavities with a cavity length of only a few wavelengths consume less power without the need for relying on ultra-high Q. This can be understood by noting that the power required by an electro-optic modulator based on free carrier dispersion to modulate a certain bandwidth will be less for a smaller cavity than a larger cavity, since the total charge required to achieve the same carrier density will be less. Therefore, decreasing the size of the device reduces the power requirement without increasing the Q of the device. In this work we demonstrate such a device with a reduced modal volume.

2. Device design and fabrication

We designed a modulator based on a compact Fabry-Pérot (F-P) resonator forming an ultra-small silicon microcavity with dimensions on the order of a few wavelengths in the material. This type of cavity was first demonstrated in silicon as a passive filter [10], showing desirable behavior as a compact filter with a large bandgap. Other works have proposed various improvements to this original structure to raise the quality factor, while also reducing insertion losses [11,12], and quality factors as high as 8900 have been experimentally demonstrated [13]. We have altered the design in [10] to create an active electro-optical device by introducing the ability to inject and extract free carriers into the cavity. A schematic of the device is shown in Fig. 1(a). The device consists of a compact F-P cavity within a single mode silicon waveguide. The cavity is formed by etching five periodic holes on either side of the cavity region that act as distributed Bragg reflectors (DBR's). These holes have diameters of 220 nm and a periodic spacing of 420 nm. The cavity at the center of the device is only 2.51 microns in length, and the entire device is less than 6 microns in length. A p-i-n diode is formed across the cavity with the presence of a thin 50 nm slab containing p+ and n+ doped regions on either side. This thin silicon slab maintains the confinement of the mode while allowing an electrical path for charge carriers to flow from the doped region into the intrinsic region at the core of the cavity. The doped regions are located

300 nm away from the waveguide to limit the interaction of the optical mode with the optically absorbing highly doped silicon regions. The Q of this specific simple geometry is approximately 780, as predicted by 3-D FDTD simulations assuming a TE-like polarization.

The high-index-contrast 450 nm wide and 250 nm tall Si-SiO_2 waveguide structure is defined on a SOI substrate using electron-beam (e-beam) lithography followed by reactive ion plasma etching (RIE) to a depth 50 nm from the buried oxide layer, leaving the thin slab which will contain the doped regions. Due to the RIE process, the holes in the DBR's do not etch to the same depth as the 50 nm slab, and are approximately 160 nm deep. The doping steps to form the p^+ and n^+ regions on either side of the micro-cavity are achieved each in order by using e-beam lithography to define a PMMA resist mask serving as an implantation barrier, followed by ion-implantation into the thin silicon slab. The p^+ implant consists of BF_2^+ with a dose of $8x10^{14}$ cm^{-2} with energy of 20 keV, while the n^+ implant consists of As^+ with a dose of $1x10^{15}$ cm^{-2} with energy of 15 keV. The device is then clad with 900 nm of SiO_2 by plasma enhanced chemical vapor deposition (PECVD). The devices are then annealed to activate the dopants, first 15 min at 900 °C for the n^+, and then 15 seconds at 1050 °C for the p^+. Following annealing steps, e-beam lithography and RIE are again used to etch vias through the cladding down to the doped regions. 15 nm of Titanium is sputtered onto the surface and annealed at 850°C for 30 second to form TiSilicide contacts with the exposed silicon. The remaining Ti is then removed and aluminum contacts are then defined using e-beam lithography and deposited by e-beam evaporation followed by lift-off. Fig. 1(b) shows an optical microscope image of a completed device displaying the waveguide and the contacts on either side of the cavity. The devices are then diced and the edge facets are polished in preparation for electro-optical characterization of the modulator's performance.
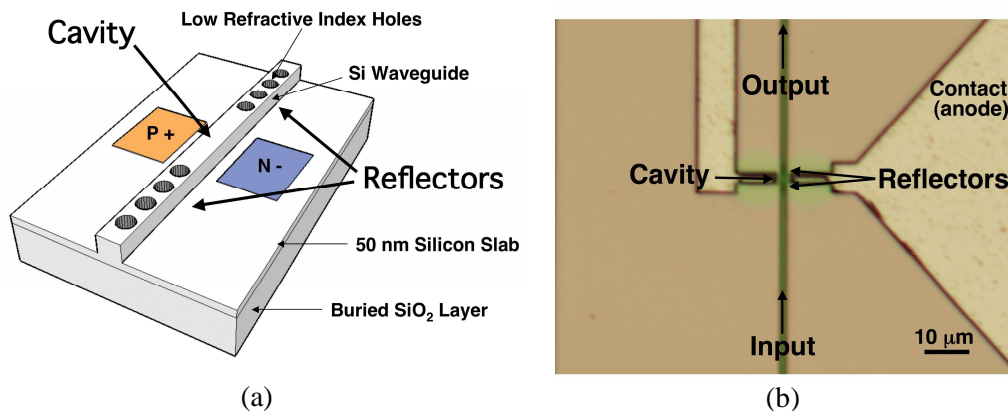

Fig. 1. (a) Schematic of the F-P modulator. The effective refractive index in the cavity is changed by carrier injection and extraction when a potential is applied across the p-i-n. (b) Optical image of a fabricated device with a cavity length of 2.51 microns on a SOI substrate, showing the metal contacts and vias on either side. The contacts are much larger than the actual doped regions. The entire device is shorter than 6 microns in length.

3. Experimental results

We have tested the performance of the modulator using both DC and AC measurements. Light was coupled into the device via a lensed fiber focused onto the facet of the input waveguide, and the output light was coupled through an objective lens through free space and into a detector. A polarization controller was used to input the TE-like polarization and a polarization filter was placed between the objective lens and detector to ensure measurement of the correct polarization. The measured spectra of the device are shown in Fig. 2 with a voltage applied that is just below the diode threshold of 0.8 V with no current flowing (solid

line), and with a larger voltage applied at 5.6 V (dashed line). The spectra in Fig. 2 have been filtered using FFT low-pass filtering to remove small F-P resonances from the spectra due to reflections at the polished input and output facets of the chip. All measurements were made with the sample mounted to a temperature controller set at 22°C in order to reduce any external thermal fluctuations. The cavity is multimode, but one resonance is present over the range of $\lambda = 1520\text{-}1620$ nm, centered at a wavelength of $\lambda = 1568.24$ nm. The cavity quality factor Q is estimated from the resonance wavelength, divided by the full-width half-maximum (FWHM) of that resonance. For the resonance centered at $\lambda = 1568.24$ nm, the measured Q of the resonator is approximately 253.2, which is somewhat smaller that the compared theoretical value of $Q = 780$. This difference in Q can be attributed to high scattering due to roughness of the sidewalls, especially in the etched holes to create the DBR's, and also to the high sensitivity of the device to the exact dimensions of these holes and the corresponding mode matching within the cavity [11]. The insertion loss into the device is estimated to be 5.1 dB estimated by comparing waveguides with and without cavities on the same chip. The total loss due to coupling in and out of the waveguide, plus the waveguide losses over 7 mm of waveguide was measured to be 21.3 +/-0.05 dB. Both of the measured spectra in Fig. 2 have been normalized to the maximum transmission of light through the device measured at a wavelength outside the bandgap at approximately $\lambda = 1490$ nm.
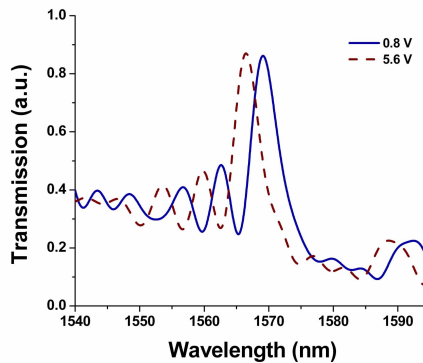

Fig. 2. Measured transmission spectrum of the micro-cavity for an applied voltage of 0.8 V (below threshold) and 5.6 V (above threshold).

The device transmission is highly sensitive to the charge injected into the cavity. The complex refractive index of the cavity is changed by applying a voltage across the anode and cathode probe pads [14]. As shown in Fig. 2, the resonance of the device is blue-shifted following the application of a voltage across the p-i-n device, decreasing the refractive index of the silicon in the cavity, as predicted by theory. Note that there is little change in the transmission or Q of the device. In an optically optimized device with a much higher cavity lifetime, carrier absorption will be noticeable, as we have measured in ring resonators. The slight increase in transmission with injected carriers is possibly due to a better mode matching between the cavity and the reflectors with the shifted effective index of the cavity. Note that some opposing thermo-optic effect is also expected due to the high resistance of the contacts (~50 kΩ), reducing the effective blue shift in these devices. The DC modulation of a single channel wavelength can be shown from dependence of the transmission on the DC bias. In Fig. 3 we show this dependence for a given wavelength of 1568.54 nm that is just above the peak resonance, normalized to the peak transmission at the resonance of 1568.24 nm. There is no change in the transmission of the optical signal for a bias below the threshold of approximately 0.8 V. A modulation as large as 5.93 dB can be achieved with an applied voltage of 5.6 V.
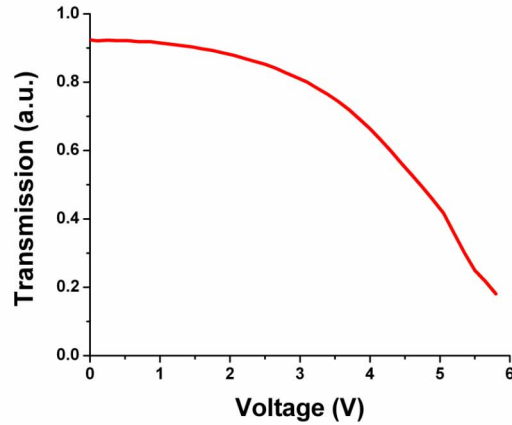
Fig. 3. Transmission as a function of applied DC bias for a wavelength of 1568.54 nm.

Electro-optical modulation of several hundreds of Mbps was achieved for a single wavelength located within the falling edge of a resonance at $\lambda = 1568.54$ nm. Fig. 4 shows an example of a transmission signal at 250 Mbps for a peak-to-peak voltage of 2.0 V with a DC bias of 0.7 V. For a peak-to-peak voltage swing of 2.0 V, a modulation of 5.87 dB can be achieved. Note that in general, the voltage required in our experiment is determined mainly by the high contact resistance, and so by improving the contact resistance the voltage required could be reduced for future devices.
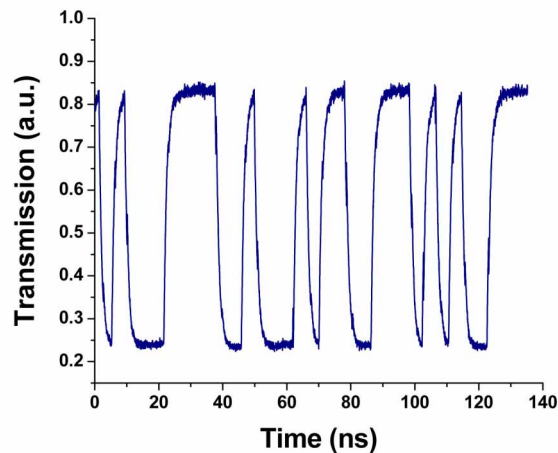

Fig. 4. Optical modulation due to an applied electrical signal at 250 Mbps.

The 10-to-90 rise time at this speed is measured to be 2.27 ns due to carrier injection and a fall time of 1.96 ns due to both carrier removal and recombination. Fig. 5 shows the maximum extinction ratio of each bit in a long continuous series of "1s" and "0s". The modulation depth quickly decreases with speed.
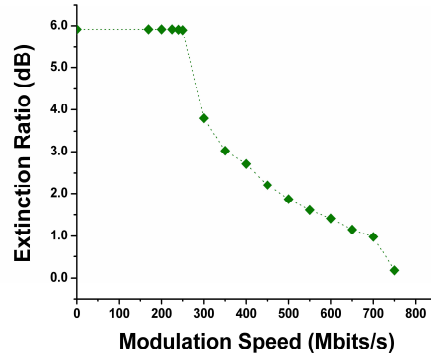
Fig. 5. Optical extinction ratio as a function of the speed of the applied AC signal.

Device simulations demonstrate that this type of small cavity can achieve higher speed modulation. The electrical modeling was carried out in SILVACO ATLAS device simulation software. The software models the internal physics of the device by solving the Poisson equation and the charge continuity equation numerically. The suitability of SILVACO for simulation of these characteristics has been established by prior works [15] and references there in. We included Shockley Read Hall (SRH), Auger, Direct recombination models. We assumed an interface trap density of $10^{10}/cm^2/eV$ and an interface recombination rate of 10^4 cm/s [15, 16]. The surface recombination rate of silicon is of the order of 10^4 cm/s for unpassivated surfaces. [17] and 100 cm/s for passivated surfaces.

Simulations of such a device predict that a fabricated structure with a quality factor matching the theoretical quality factor of the device should be able to achieve modulation speeds of 1 Gbps assuming the current DC electrical characteristics of the fabricated device as shown in Fig. 6(a), assuming a DC bias of 0.3 V. If optimized for higher Q's [11-13], similar size or smaller cavities could produce speeds of 10 Gbps with Q's of 10,000. This is shown in Fig. 6(b), where we compare the relative rise and fall times that can be achieved for the case of a Q=780 as predicted for the current geometry with Q's of 10,000 and 20,000. This plot assumes ideal electrical performance with reduced contact resistance (5 kΩ) as compared to the fabricated devices.

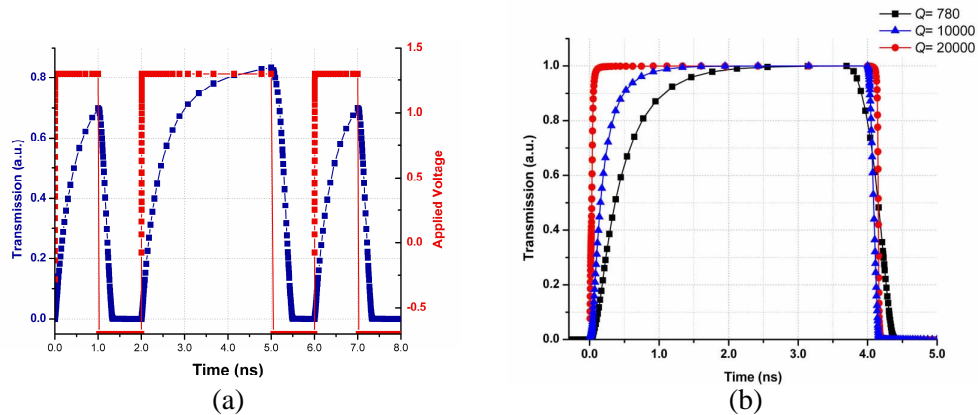(a)   (b)

Fig. 6. (a) Simulated 1 GBPS operation for the present device with Q=780, voltage swing of 2.0 V and DC bias of 0.3 V. (b) Simulated rise and fall times for electrically ideal p-i-n structures with different Q's.

4. DC comparison and analysis of modulators

The advantage smaller devices provide is clear by comparing the performance of larger ring resonator modulators fabricated on the same platform [18] with the ultra-small F-P resonator cavities. For a homogenous refractive index change in a silicon cavity due to the plasma dispersion effect, Δn_{cavity} can be described as

$$\Delta n_{cavity} = -[8.8 \times 10^{-22} \bullet (\Delta N_e) + 8.5 \times 10^{-18} \bullet (\Delta N_h)^{0.8}] \qquad (1)$$

where ΔN_e and ΔN_h are the concentration of electrons and holes in Silicon [7]. The change in the refractive index of the cavity, for a given cross section (such as the one used for both ring resonators in [8] and the ultra-small cavity discussed here) can be approximated as

$$\Delta n_{cavity} \propto \frac{P}{AL} \qquad (2)$$

where P is the power required to maintain a certain number of steady-state absolute carriers in a given geometry, which is directly related to the length L of the device at a certain carrier concentration for a given cross-sectional area A. This assumes that the carrier-lifetime in both cases is similar as measured in similar devices fabricated on the same platform for all-optical switching [19,20]. The approximate modulation depth MD is then given by

$$MD \propto \frac{\Delta\lambda_{resonance}}{\delta\lambda_{FWHM}} \propto \frac{Q \bullet P}{AL} \qquad (3)$$

where $\Delta\lambda_{resonace}$ is the absolute shift of the resonance peak, and $\delta\lambda_{FWHM}$ is the full-width half-maximum of the resonance, which is a measure of the bandwidth of the device. Q is the quality factor of the resonator. This proportionality does not include the shape of the resonance, which would determine the exact value of the modulation depth.

A figure of merit for these modulators is the total amount of bandwidth desired at a certain modulation depth, and the power required to do so. Noting that the modulation depth is proportional to the Q, while the bandwidth is inversely proportional to the Q using this figure of merit (FOM) and equation (3)

$$FOM = \frac{MD \times Bandwidth}{Power} \propto \frac{1}{V_{eff}} \qquad (4)$$

where V_{eff} is the effective volume of the refractive index changing cavity region, which is simply AL. Therefore this figure of merit improves as $1/V_{eff}$.

The linear Fabry-Pérot cavity shown here, with a cavity length of only 2.51 microns, has a V_{eff} of $3.4 \bullet (\lambda/n_{eff})^3$, which is less than that of even a small 10 micron diameter ring resonator, which has a V_{eff} that is $42.6 \bullet (\lambda/n_{eff})^3$. The absolute change in effective refractive index, and therefore the absolute wavelength change, depends on the power consumed and the size of the cavity as shown in equation 4. Therefore, for a given power the absolute shift will increase with smaller cavities. This is shown experimentally in Fig. 7, where the wavelength shift from one of our F-P cavities is much greater compared to the same power in a ring resonator that were fabricated together on the same platform, assuming similar contact resistance for both types of devices. For a power of 1850 µW a total shift in a small 10 µm diameter ring is only 1 nm, while in the small F-P cavity it is as large as 3.5 nm for the same power. Shifts of 4.1 nm have been measured in this F-P cavity, which is a shift unattained using the rings. As the current increases inside the ring the depth of the resonance in the rings drops due to carrier absorption in the higher Q cavity, so that above powers of 2000 µW the resonance is

extremely shallow, while at the same input power the lower-Q F-P cavity is barely affected. Note that smaller ring resonators have been demonstrated [21], but they still have larger cavity volumes than those possible using 1-D cavities such as the one we have demonstrated.
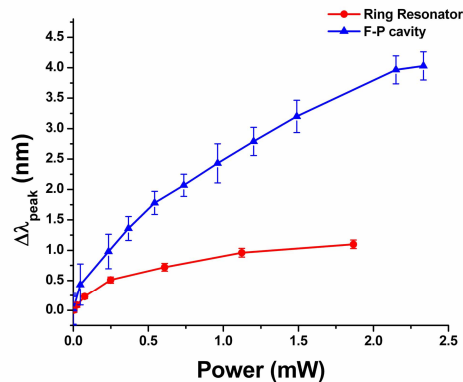

Fig. 7. Absolute shift in the peak resonance as a function of the DC power consumed in the device for a ring resonator (circumference = 31.4 μm) and a F-P cavity (length of 2.51 μm).

Using a smaller device enable high performance with low power, relaxing the requirements for high Q's resonators. One advantage that low Q resonators offer, in addition to enabling transmission at higher data rates as discussion above, is a reduction in temperature sensitivity. Since a lower Q modulator requires a larger absolute shift in the resonance, temperature variations will have a reduced effect on the modulation since a given temperature change only effects the absolute shift in the resonance. When compared to longer cavities with the same cross-section and effective index, the lower Q cavity will have a reduction in sensitivity proportional to the ratio of the Q of the devices. For example, relative to ring resonator modulators [8], using the F-P device one can achieve approximately two orders of magnitude reduction in temperature sensitivity. The experimentally measured sensitivity $d\lambda/dT$ for the F-P cavities is 0.0935 +/- 0.0015 nm/°C, which is small relative to the FWHM of 6.3 nm, while for a 10 micron diameter ring the measured sensitivity of 1.3045 +/- 0.0012 nm/°C is large compared to the much smaller FWHM of 0.025 nm. Another advantage provided by this relaxed requirement is that a wider resonance peak will provide a wider spectral bandwidth of closely-spaced channels that can be shifted with the same device. This could be expanded again by using coupled resonator cavities to expand and shape the profile of transmission spectrum, while the combined size of several smaller devices could still be smaller than a single large cavity.

5. Conclusion

In conclusion we demonstrate an ultra-compact electro-optic modulator for dense integrated photonic and interconnect applications that is CMOS compatible. The figure of merit of bandwidth/power is improved by reducing the size of the device, as shown by comparing these small devices to larger ring resonators. By optimizing both the optical confinement of small cavities and the electrical performance, smaller and lower power modulators with GHz speeds may be realized while relaxing the requirement of high Q microcavities.

Acknowledgments